

# Y<sub>2</sub>Zr<sub>2</sub>O<sub>7</sub> (YZ)-pyrochlore based oxide as an electrolyte material for intermediate temperature solid oxide fuel cells (ITSOFCs)—Influence of Mn addition on YZ

M. Kumar<sup>a</sup>, I. Arul Raj<sup>b,\*</sup>, R. Pattabiraman<sup>b</sup>

<sup>a</sup> National Metallurgical Laboratory, CSIR Madras Complex, Chennai, India

<sup>b</sup> Central Electrochemical Research Institute, Karaikudi, India

Received 20 March 2007; received in revised form 7 September 2007; accepted 14 September 2007

## Abstract

Compositions in the pyrochlore system Y<sub>2</sub>Zr<sub>2</sub>O<sub>7</sub> (YZ) and Y<sub>2</sub>Zr<sub>2-x</sub>Mn<sub>x</sub>O<sub>7-δ</sub> (YZM) (where  $x = 0.025, 0.05, 0.075$  and  $0.10$ ) were examined as possible alternatives to stabilised zirconia solid oxide electrolyte in intermediate temperature solid oxide fuel cells (ITSOFC). Such materials were prepared by glycine–nitrate combustion process. The prepared compounds were characterised by X-Ray Diffraction and Thermal analysis. Circular pellets were fabricated and annealed at different temperatures ranging from 1000 to 1400 °C. The sintering behaviour of YZ and YZM were investigated to obtain information on the densification factor, relative percentage shrinkage/expansion in volume after heat treatment and apparent porosity value. The small doping level of Mn ( $\leq 10.0$  wt%) resulted in increased conductivity values. The component diffusion coefficients and mobility of ions are calculated from its conductivity value.  $D_{\text{comp}}$  and  $\mu_i$  are found in the range of  $10^{-8}$  cm<sup>2</sup> s<sup>-1</sup> and  $10^{-7}$  cm<sup>2</sup> V<sup>-1</sup> s<sup>-1</sup>, respectively. The key features, which make the YZ and YZM systems attractive as a fuel cell electrolyte, are discussed. © 2007 Elsevier B.V. All rights reserved.

**Keywords:** Yttrium zirconate pyrochlore oxides; Combustion method; Sintering studies; Scanning electron microscope; Conductivity measurements

## 1. Introduction

Ytria-stabilised zirconia (YSZ) is generally used as an electrolyte material for solid oxide fuel cell (SOFC) because of its good mechanical strength and high stability under oxidizing and reducing atmosphere at high temperatures [1,2]. The YSZ electrolyte usually has to be operated at about 1000 °C, where the ionic conductivity reaches the required high level. However, such high temperatures lead to a high fabrication cost and degradation of cell components. To reduce the operating temperature of the SOFC system, much attention has been paid recently to investigate alternate electrolyte materials such as partially substituted lanthanum gallate, ceria and also pyrochlore type oxide materials (Y<sub>2</sub>Zr<sub>2</sub>O<sub>7</sub>, yttrium zirconate (YZ)). Rare earths based pyrochlore oxides exhibiting high ion conductivity have been reported [3–12]. It has also been reported that at low doping levels, the addition of Mn/Fe or Co enhances the conductivity of the material [13–15]. It is desirable in this context to

determine whether higher doping levels might yield yttrium zirconate based compositions exhibiting adequate conductivity for use as materials for components in ITSOFCs [16]. The present study is under taken to determine the effect of partially substituting Mn/Fe or Co on Zr-site in Y<sub>2</sub>Zr<sub>2</sub>O<sub>7</sub> in comparison with Y<sub>2</sub>Zr<sub>2</sub>O<sub>7</sub>.

## 2. Experimental

The yttrium zirconate and Mn-doped yttrium zirconate were prepared by combustion synthesis process using glycine as a fuel [17]. The combustion method involves the combustion of saturated aqueous solution containing stoichiometric quantities of the corresponding nitrates (oxidizers) and glycine (fuel). The appropriate quantities of the precursor nitrate salts (if oxide/acetate salts were taken, they were converted as nitrates by treating them with nitric acid) were calculated according to the concepts of propellant chemistry [18,19]. The oxidizer and fuel ratio was calculated based on oxidizing and fuel valencies of the reactants keeping  $O/F = 1$  as reported [20,21]. The aqueous redox solution containing metal nitrates and glycine when introduced into a muffle furnace preheated to 823 K, boils, froths, ignites and catches fire (at a high temperature 1373 K). At this temperature the metal nitrates decompose to metal oxides and oxides of nitrogen and hence act as oxidizer for further combustion, which leads to voluminous, foamy combustion residue in less than 5 min. The as-synthesised powders were calcined at 1073 K for 6 h in air

\* Corresponding author. Tel.: +91 4565 227552; fax: +91 4565 227779.  
E-mail address: [iarulraj@rediffmail.com](mailto:iarulraj@rediffmail.com) (I.A. Raj).

to remove the deposited carbon and unreacted organic residues to get a pure compound.

### 3. Characterisation

The phase purity of YZ and Mn-doped YZ powder was identified through X-ray diffraction technique using Cu K $\alpha$  radiation in JEOL X-ray Diffractometer (model 8030). The bulk density, tap density and absolute density values were determined by the Archimedes method using xylene as medium. The sintering behaviour of these materials was also investigated. The microstructures of the gold sputtered (JEOL Fine Coat Ion Sputter JFC-1100) annealed samples were investigated by SEM (S-3000 H, Hitachi Scanning Electron Microscopy at an acceleration voltage of 20 kV). Thermo-gravimetric analysis (TGA) was performed in air on powder specimens using heating and cooling rates of 10 °C min<sup>-1</sup>. The conductivity measurements on YZ and partially Mn-doped YZ pellets were carried out in air using ac impedance spectroscopy in the frequency ranging from 100 Hz to 100 KHz as a function of temperature.

## 4. Results and discussion

### 4.1. X-ray diffraction

The XRD pattern of the parent YZ and partially 10 wt% Mn-doped YZ are shown in Fig. 1. The *d*-values obtained are in agreement with the formation of pyrochlore phase as reported [20]. However, the JCPDS data files corresponding to the partially substituted pyrochlore oxides are not available for comparison.

By using Scherrer equation, the average crystallite size of the YZ and doped YZ materials are calculated from the broadening of a specific diffraction peak. The equation is given below,

$$d = 0.9 \frac{\lambda}{\beta} \cos \theta$$

where *d* is the average size of the crystallite. 0.9 is Scherrer constant,  $\lambda$  is the wavelength of radiation,  $\beta$  is the peak width at half and  $\theta$  corresponds to the peak position. The results of this analysis are given in Table 1. It reveals that the densification of the YZ pyrochlore compound at high temperature is less. Because of smaller crystallite size, the material has larger surface free energy [22]. Generally, the reduction of surface free energy is the driving force for sintering of the material [23] which is the reason for the low densification of YZ at high temperature.

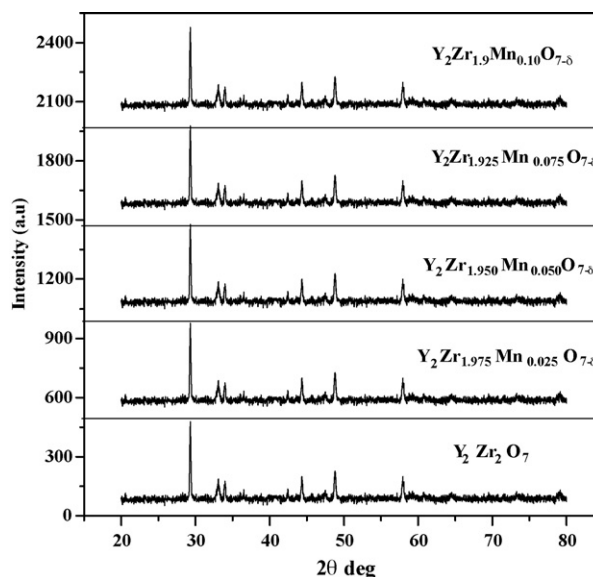


Fig. 1. XRD pattern of Y<sub>2</sub>Zr<sub>2</sub>O<sub>7</sub> and partially Mn-doped YZ.

### 4.2. Particulate properties

#### 4.2.1. Density measurement

The bulk, tap and absolute density values (measured using a pycnometer with xylene liquid) of Y<sub>2</sub>Zr<sub>2</sub>O<sub>7</sub> and Mn-doped Y<sub>2</sub>Zr<sub>2</sub>O<sub>7</sub> powder were obtained and are given in Table 2. From the density data, it is drawn that the synthesised powders are fluffy and fine in nature.

#### 4.2.2. Sintering studies

The synthesised materials were uni-axially pressed into circular components at an axial stress of 256 MPa by taking the powders in a die using hydraulic pressing machine for 2 min duration. The circular components were subjected to annealing at different temperatures ranging from 1273 to 1773 K in a computer controlled programmable furnace at a heating and cooling rate of 20 °C min<sup>-1</sup> for 3 h. The densification factors were calculated from the dimensions of the green and sintered compact. The apparent porosity values were also measured for the sintered components as a function of sintering temperature by a liquid adsorption method using dioxan medium. The densification factor and porosity values are given in Table 3. The percentage theoretical density values as function of temperature is shown in Fig. 2.

Table 1

The crystallographic data of Y<sub>2</sub>Zr<sub>2</sub>O<sub>7</sub> and Mn-doped Y<sub>2</sub>Zr<sub>2</sub>O<sub>7</sub> powders

Sample	Crystal structure	Unit cell parameter (Å)	Unit volume (Å <sup>3</sup> )	Theoretical density (g cc <sup>-1</sup> ) $\rho = ZM/N \times V$	Crystallite size (nm)
YZ	Defect fluorite	10.474	1149.05	5.459	3.782
2.5% Mn in YZ	Defect fluorite	10.469	1147.40	5.456	10.798
5.0% Mn in YZ	Defect fluorite	10.467	1146.75	5.449	12.368
7.5% Mn in YZ	Defect fluorite	10.462	1145.10	5.446	15.124
10% Mn in YZ	Defect fluorite	10.461	1144.77	5.430	11.092

Table 2  
The density data of yttrium zirconate and Mn-doped yttrium zirconate powders

Wt% Mn in YZ	Bulk density (g cc <sup>-1</sup> )	Tap density (g cc <sup>-1</sup> )	Absolute density (g cc <sup>-1</sup> )
0.00	0.165	0.3056	2.403
2.50	0.196	0.3629	2.548
5.00	0.210	0.4375	3.135
7.50	0.184	0.3538	3.135
10.0	0.197	0.4104	3.581

Table 3  
The effect of temperature on percentage of theoretical density and porosity of Y<sub>2</sub>Zr<sub>2</sub>O<sub>7</sub> and Mn-doped Y<sub>2</sub>Zr<sub>2</sub>O<sub>7</sub>

T (K)	Y <sub>2</sub> Zr <sub>2</sub> O <sub>7</sub> (YZ)		2.5% Mn in YZ		5.0% Mn in YZ		7.5% Mn in YZ		10.0% Mn in YZ	
	% T.D.	% P	% T.D.	% P	% T.D.	% P	% T.D.	% P	% T.D.	% P
1273	49.62	61.55	48.75	67.99	47.37	75.65	48.16	57.04	48.40	51.31
1373	49.70	58.16	46.75	70.73	51.27	66.27	49.59	62.73	51.25	47.55
1473	49.88	53.47	50.91	67.94	51.73	64.51	52.19	60.87	52.04	50.73
1573	50.60	42.33	60.41	58.43	54.00	58.72	57.70	51.93	63.75	45.72
1673	59.70	33.00	68.77	31.02	69.85	37.78	70.67	30.57	72.23	30.63
1773	77.29	8.72	77.58	30.09	78.0	27.81	80.0	28.70	75.0	28.57

#### 4.3. Thermo-gravimetric analysis

The results from TGA in air are shown in Fig. 3. The compositions such as YZ parent pyrochlore and partially 10% Mn-doped YZ which exhibited a reversible weight loss when heated in air. The weight loss results from the loss of lattice oxygen as the materials become increasingly oxygen deficient with increasing temperature. Similar behaviour has been observed in perovskite containing Co or Fe [16]. Since electro neutrality must be maintained within a crystalline material, the oxygen valencies created

by the loss of lattice oxygen must be charge compensated by other changes within the crystal. Mn adopts a number of valence states, while Y and Zr in YZ are essentially fixed valence states, so the oxygen vacancies are almost certainly compensated through reduction in valence of some of the Mn. This temperature dependent oxygen stoichiometry has an effect on the electrical behaviour of these materials.

#### 4.4. Scanning electron microscopy

The morphology of yttrium zirconate and Mn-doped yttrium zirconate (2.5%, 5.0%, 7.5% and 10.0%), which were sintered

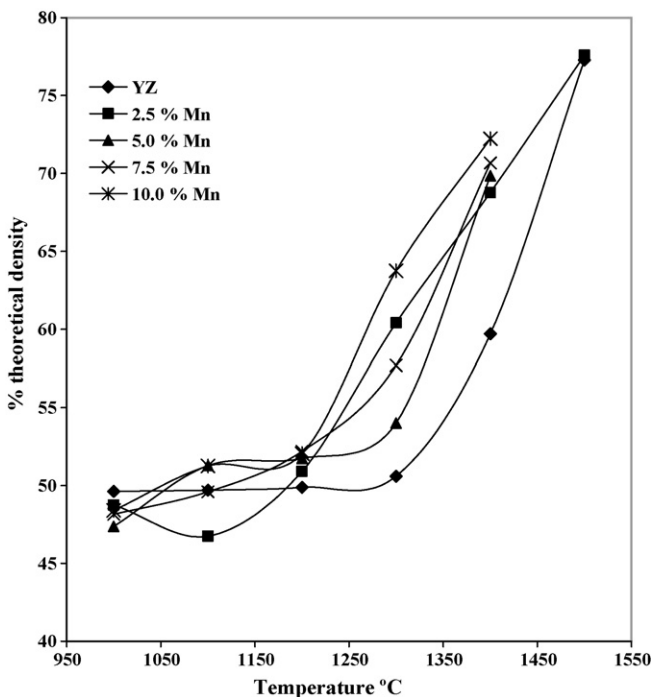


Fig. 2. The effect of temperature on % theoretical density of YZ and partially Mn-doped YZ.

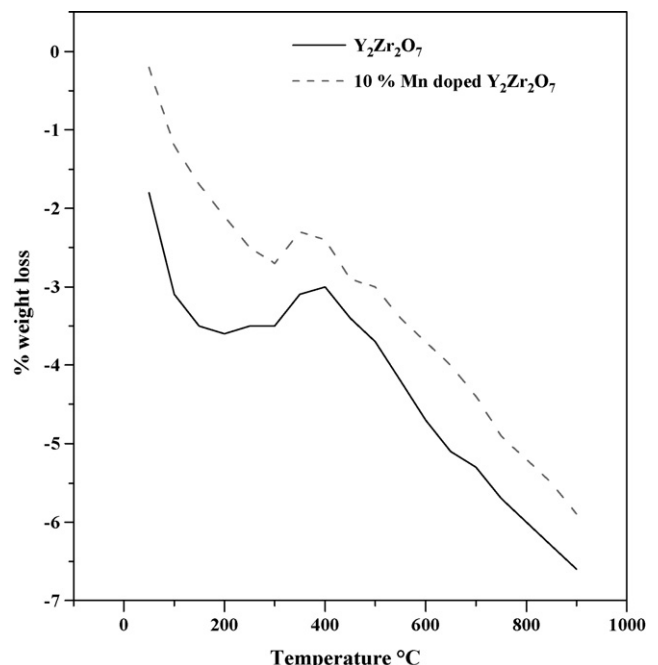


Fig. 3. TGA pattern of YZ and partially 10 mol% Mn-doped YZ.

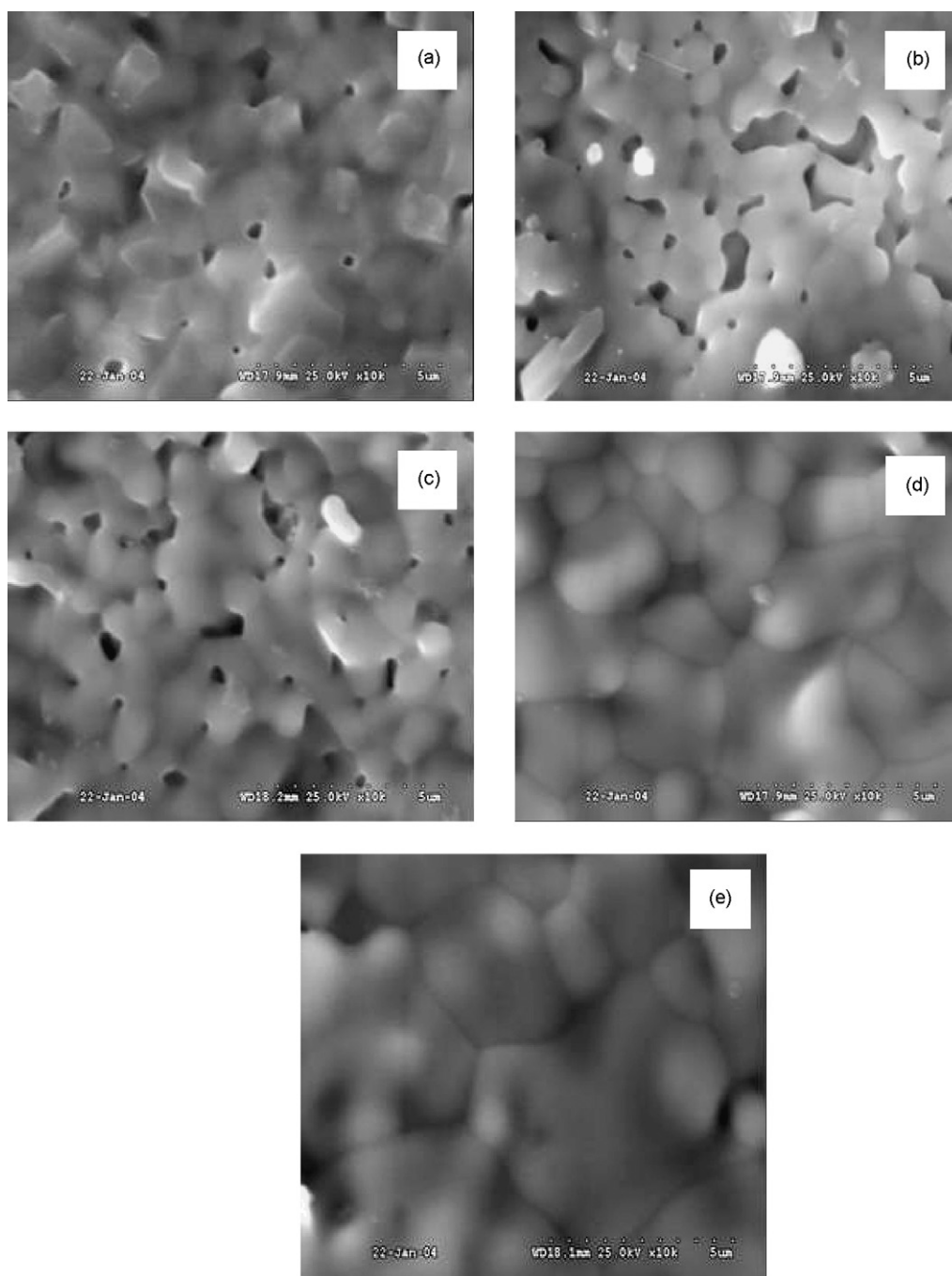


Fig. 4. The morphology of (a)  $\text{Y}_2\text{Zr}_2\text{O}_7$ , (b) 2.5 mol% in  $\text{Y}_2\text{Zr}_2\text{O}_7$ , (c) 5.0 mol% in  $\text{Y}_2\text{Zr}_2\text{O}_7$ , (d) 7.5 mol% in  $\text{Y}_2\text{Zr}_2\text{O}_7$  and (e) 10.0 mol% in  $\text{Y}_2\text{Zr}_2\text{O}_7$ .

at 1773 K are shown in Fig. 4a–e, respectively. The effectiveness of Mn addition Zr-site in yttrium zirconate is also evident from the SEM micrograph of the sintered specimens as shown in Fig. 4b–e. A progressive change in microstructure with Mn addition is clearly visible. Fig. 4a shows grains with small pores in the structure but pore size increases with small addition of Mn content, is shown Fig. 4b and c. In the case of higher addition of Mn on Zr-site in  $\text{Y}_2\text{Zr}_2\text{O}_7$ , it was found that there are no pores and it shows a perfect grain boundary, which is shown in Fig. 4d and e.

#### 4.5. Conductivity measurements

The bulk conductivity of YZ and Mn-doped YZ were measured by a two-probe ac impedance technique. The bulk conductivity has been measured in the range of temperature 500–800 °C.

In general, the ac impedance of an ionic conductor measured by a two-probe method contains contribution from the bulk, grain boundaries and electrode/electrolyte interface, which can be reflected in a complex plane by three successive arc,

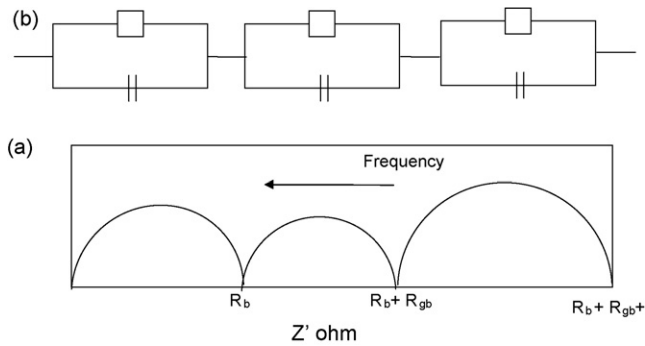


Fig. 5. An idealised equivalent circuit (b) and its corresponding impedance plot (a).  $C_b$ ,  $R_b$  and  $C_{gb}$ ,  $R_{gb}$  and  $C_{el}$ ,  $R_{el}$  represents resistance and capacitance for bulk, grain boundary and electrode process, respectively.

as shown in Fig. 5a. The frequency increases from the right to the left across the plot. The arc at the high frequency end of spectrum represents the bulk resistivity; the arc at the middle is a consequence of the grain boundary effects; the low frequency arc is assigned to the electrode response. An idealised equivalent circuit for the ceramic oxides corresponding to the impedance plot is shown in Fig. 5b. In a practical case, however, not all these arcs can be observed, depending on the nature of the samples and testing conditions.

The conductivity values obtained on YZ and Mn-doped YZ are shown in Fig. 6. The bulk conductivity values were measured and the energy of activation of YZ and partially Mn-doped YZ were calculated and given in Table 4.

Fig. 6 shows that the conductivity values of partially Mn-doped YZ increases as a function of temperature. The energy of activation values was obtained and it was found that the increase in the conductivity values for the 5 and 10 wt%. Mn substituted

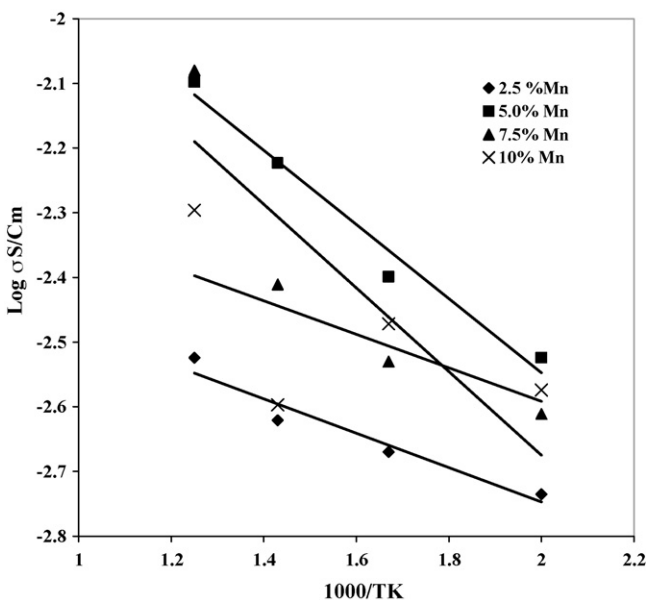


Fig. 6. The effect of temperature on conductivity values of partially Mn-doped YZ.

Table 4

The conductivity values of  $Y_2Zr_2O_7$  and Mn-doped  $Y_2Zr_2O_7$  materials

$T$ (K)	Conductivity $\times 10^{-3}$ S $cm^{-1}$				Ea kJ (1073 K)
	773 (K)	873 (K)	973 (K)	1073 (K)	
0% Mn	1.77	1.99	2.50	3.75	-7.261
2.5% Mn	1.84	1.99	2.391	2.989	5.228
5.0% Mn	2.989	3.986	5.979	7.972	10.970
7.5% Mn	2.451	2.948	3.881	8.317	12.375
10.0% Mn	2.668	3.369	2.526	5.053	4.961

YZ can be attributed to not only ion migration in the lattice but also the defect formation arising due to Mn substitution for Zr [24].

Component diffusion coefficient and mobility of ions of those materials were calculated from conductivity values of YZ and partially Mn-doped YZ. The component diffusion coefficient  $D_{comp}$  is a gradient which acts as driving force for the migration of specified component. Migration of ions in solid electrolyte under electric field is an example of this diffusion. The equation for the mobility of ions is given as follows,

$$\mu_i = \frac{\sigma}{Nq}$$

The concept of  $D_{comp}$  is very important for the solid electrolyte since it is related to conductivity,  $\sigma$  with Nernst–Einstein equation, given as

$$\sigma = \frac{Z^2 en D_{comp}}{KT}$$

The values of  $D_{comp}$  for mobile ions in good solid electrolytes can be higher than  $1 \times 10^{-8}$   $cm^2 s^{-1}$ . but we found that the obtained component diffusion coefficient is close to the reported value. The  $D_{comp}$  and  $\mu_i$  are shown in Table 5. From the table, it is seen that the YZ and partially Mn-doped YZ are having same order of diffusion coefficients. This means that the surface reaction (e.g., adsorption of oxygen) is not rate limiting during the oxygen uptake in this kind of materials [25].

Table 5

$D_{comp}$  and  $\mu_i$  of  $Y_2Zr_2O_7$  and partially Mn-doped  $Y_2Zr_2O_7$

$T$ ( $^{\circ}C$ )	$D_{comp} \times 10^{-8}$ $cm^2 s^{-1}$ for various wt% level of Mn-doped YZ			
	2.5	5	7.5	10
500	0.3722	0.6046	0.4958	0.5396
600	0.4559	0.9105	0.6734	0.7696
700	0.6087	1.522	0.9881	0.6431
800	0.8392	2.4215	2.3351	0.6431
$T$ ( $^{\circ}C$ )	$\mu_i \times 10^{-7}$ $cm^2 V^{-1} s^{-1}$ for various wt% level of Mn-doped YZ			
	2.5	5	7.5	10
500	0.5589	0.9074	0.7445	0.8104
600	0.6063	1.2107	0.8954	1.0234
700	0.7263	1.8162	1.1789	0.7673
800	0.9079	2.4215	2.5263	1.5348

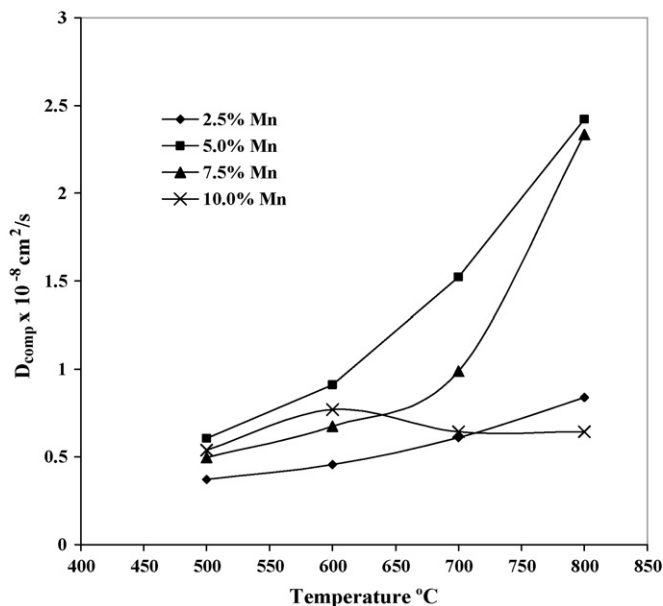


Fig. 7. The effect of temperature on component diffusion coefficient of partially Mn-doped YZ.

The effects of temperature on component diffusion coefficient and ionic mobility are shown in Figs. 7 and 8, respectively. It is found that the behaviours are similar when compared with conductivity plots of YZ and partially Mn-doped YZ, i.e., the lower value of the mobility of ions and component diffusion coefficients show lower conductivity for all compositions. The  $D_{\text{comp}}$  and  $\mu_i$  values increase with temperature. The correlation between the obtained conductivity, mobility of ions and diffusion coefficients at 800 °C is shown in Fig. 9. It is observed that there exists a linear relationship among these critical experimental parameters.

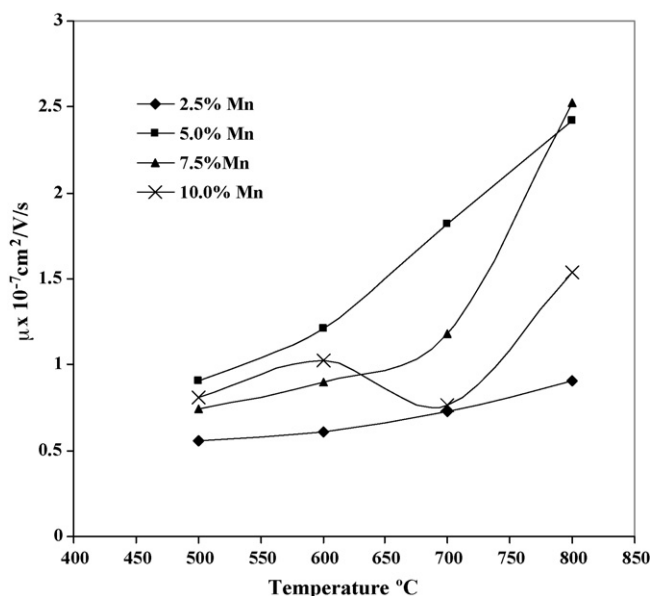


Fig. 8. The effect of temperature on mobility of ions for partially Mn-doped YZ.

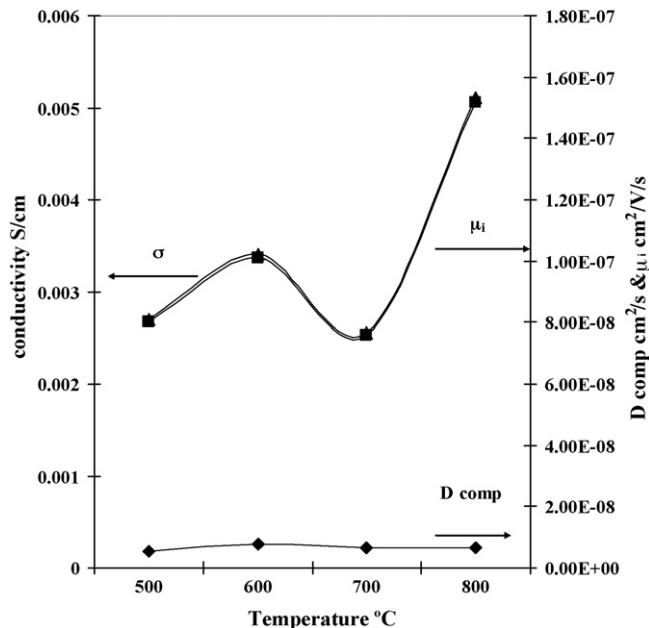


Fig. 9. The correlation between conductivity, mobility of ions and component diffusion coefficient with respect to temperature for partially 10% Mn-doped YZ.

## 5. Conclusion

$\text{Y}_2\text{Zr}_2\text{O}_7$  doped with Mn on the B-site exhibited a wide range of electrical and thermal behaviour. For relatively small additions of Mn, the bulk conductivity increased at low temperatures (due to the introduction of electronic charge carriers into the lattice), but at high temperature, the conductivity was dominated by ionic conduction. The thermal behaviour of YZ and partially Mn-doped YZ are brought out from the steady state sintering experiments to draw useful information on the dependence of % shrinkage in volume and the % theoretical density with respect to the apparent % porosity values for the first time. The conductivity values measured for these  $\text{Y}_2\text{Zr}_2\text{O}_7$  compositions in this study ( $8.3 \times 10^{-3} \text{ Scm}^{-1}$ ) is much lower than the traditional electrolytes. However, when fabricated as thin, dense and compact layers in thickness values ranging 20–50  $\mu\text{m}$  as in the case of traditional electrolytes, there is a possibility to realise higher conductivity levels which will enable them to be used as alternate electrolyte material with Ni–YZ cermet anode in intermediate temperature SOFCs. The component diffusion coefficients and mobility of ions are calculated from conductivity values.  $D_{\text{comp}}$  and  $\mu_i$  are found to be in the range of  $10^{-8} \text{ cm}^2 \text{ s}^{-1}$  and  $10^{-7} \text{ cm}^2 \text{ V}^{-1} \text{ s}^{-1}$ , respectively. The values of  $D_{\text{comp}}$  for mobile ions in good solid electrolytes can be higher than  $1 \times 10^{-8} \text{ cm}^2 \text{ s}^{-1}$ , and the  $D_{\text{comp}}$  value we obtained for the  $\text{Y}_2\text{Zr}_2\text{O}_7$  is in the same order  $1 \times 10^{-8} \text{ cm}^2 \text{ s}^{-1}$ .

## Acknowledgements

The authors are grateful to the Department of Science and Technology, New Delhi for the financial support through SERC Scheme. The authors are also thankful to the Director, CECRI, Karaikudi for his interest in this work.

**References**

- [1] A. Nakamura, J.B. Wagner Jr., *J. Electrochem. Soc.* 127 (1980) 2325.
- [2] K.J. Verker, B.J. Middelhuis, A.J. Burggraaf, *Solid State Ionics* 6 (1982) 159.
- [3] M. Kumar, A. Samson Nesaraj, I. Arulraj, R. Pattabiraman, *Seventh International Symposium on Advances in Electrochemical Science and Technology*, November 27–29, Chennai, India, 2002.
- [4] M. Kumar, M. Anbu Kulandainathan, I. Arulraj, R. Chandrasekaran, R. Pattabiraman, *Mater. Chem. Phys.* 92 (2005) 303.
- [5] R. Doshi, Von L. Richards, J.D. Carter, X. Wang, M. Krumpelt, *J. Electrochem. Soc.* 146 (1999) 1273.
- [6] A.J. Burggraaf, T. Van Dijk, M.J. Verkerk, *Solid State Ionics* 5 (1981) 519.
- [7] M.P. Van Dijk, K.J. de Vries, A.J. Burggraaf, *Solid State Ionics* 9 (1983) 913.
- [8] M.P. Van Dijk, A.J. Burggraaf, A.N. Cormack, C.R.A. Catlow, *Solid State Ionics* 17 (1985) 159.
- [9] T. Moriga, A. Yoshiasa, F. Kanamaru, K. Koto, *Solid State Ionics* 31 (1989) 319.
- [10] A.K. Shukla, J. Gopalakrishnan, *Bull. Mater. Sci.* 11 (1995) 109.
- [11] P.K. Moon, H.L. Tuller, in: S.C. Singhal (Ed.), *Proceedings of the First International Symposium on Solid Oxide Fuel Cells*, vol. 89–11, The Electrochemical Society, New York, 1989, p. 30.
- [12] S. Kramer, M. Spears, H.L. Tuller, in: S.C. Singhal, H. Iwahara (Eds.), *Proceedings of the Third International Symposium on Solid Oxide Fuel Cells*, vol. 93–4, The Electrochemical Society, New York, 1993, p. 119.
- [13] T. Ishihara, T. Akbay, H. Furutani, Y. Takita, *Solid State Ionics* 113–115 (1998) 585.
- [14] T. Shibayama, T. Ishihara, M. Handa, H. Furutani, Takita, in: *Fuel Cells Seminar Abstracts Associates*, 1998, Washington, 1998, p. 442.
- [15] A. Daidouh, C. Pico, M.L. Veiga, A. Almontassir, M. Abboudi, L. Hanebali, *Solid State Sci.* 6 (2004) 71.
- [16] J.W. Stevenson, K. Hasinska, N.L. Canfield, T.R. Armstrong, *J. Electrochem. Soc.* 147 (2000) 3213.
- [17] J. Stevenson, T. Armstrong, D. McCready, L. Pederson, W. Weber, *J. Electrochem. Soc.* 144 (1997) 3613.
- [18] T. Mimani, *Resonance* 5 (2000) 50.
- [19] R.D. Purohit, A.K. Tyagi, M.D. Mathews, S. Saha, *J. Nuclear Mater.* 280 (2000) 50.
- [20] N. Arul Dhas, K.C. Patil, *J. Mater. Chem.* 3 (1993) 1289.
- [21] L.E.I. Frah, M. Massor, M. Lemal, C. Julien, S. Chitra, P. Kalyan, T. Mohan, R. Gangadharan, *J. Electroceram.* 3–4 (1999) 425.
- [22] A.K. Bhattachaya, A. Hartridge, K.K. Mallick, J.L. Woodhead, *J. Mater. Sci.* 29 (1994) 6076–6078.
- [23] D. Segal, in: *Chemistry of Solid State Materials*, Cambridge University Press, Cambridge, 1985, p. 23.
- [24] V.V. Kharton, I.P. Marozau, N.P. Vyshatko, A.L. Shaula, A.P. Viskup, E.N. Naumovich, F.M.B. Marques, *Mater. Res. Bull.* 38 (2003) 773.
- [25] S. Yamaguchi, K. Kobayashi, K. Abe, S. Yamazaki, Y. Iguchi, *Solid State Ionics* 113–115 (1998) 393.